JOC The Journal of Organic Chemistry

ARTICLE

pubs.acs.org/joc

Incorporating BODIPY Fluorophores into Tetrakis(arylethynyl)benzenes

Daniel T. Chase, Brian S. Young, and Michael M. Haley*

Department of Chemistry and Materials Science Institute, University of Oregon, Eugene, Oregon 97403-1253, United States

Supporting Information

ABSTRACT: Six structural isomers of a tetrakis(arylethynyl)-benzene (TAEB) chromophore functionalized with dibutylamine and BODIPY moieties as the corresponding donor and acceptor units were prepared. To evaluate the effectiveness of the donor group, two TAEB molecules and three structurally related bis(arylethynyl)benzene (BAEB) isomers containing only acceptors were also synthesized. The electronic absorption and emission spectra of each series were examined. Additionally, computational studies were employed to corroborate the relative energy levels and gaps present in each series.

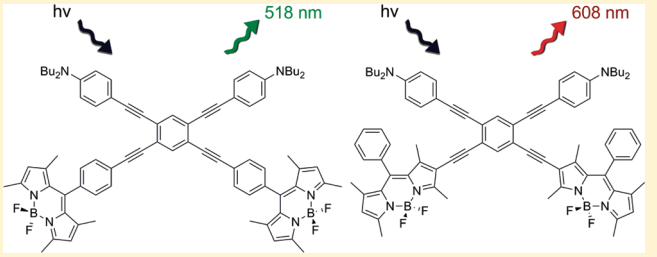

INTRODUCTION

Highly conjugated, carbon rich molecules are of great interest due to their unique optoelectronic properties.[1] These molecules are now recognized as suitable materials for advanced applications such as light-emitting diodes, photovoltaics, and thin film transistors.[2] Over the last several years, we have described detailed structure−property relationship studies on donor/acceptor-functionalized tetrakis(arylethynyl)benzenes (TAEBs).[3] These cruciform-shaped molecules possess multiple pathways for electronic and photonic transfer and are amenable to a host of substitution patterns (Figure 1). We and others[4] have shown that the band gap of these molecules can be tuned with a high degree of sensitivity with judicious choice of the nature and substitution motif of the donor and acceptor units, thereby enhancing their optical and nonlinear optical (NLO) properties. Additionally, these molecules have aptly demonstrated their ability to act as ionic sensors through dynamic shifting of their emission spectra through stepwise intramolecular charge-transfer, as evidence of fine control over their HOMO and LUMO energy levels.[5]

To further explore the potential of the TAEB system, we sought out a stronger acceptor in an effort to increase charge transfer, as seen by a stronger net dipole, and therefore to exhibit a larger bathochromic shift into the red region. To meet these criteria, we employed the 4,4-difluoro-4-bora-3a,4a-diaza-s-indacene core, better known as BODIPY, as our acceptor unit. The BODIPY moiety has garnered a significant amount of attention due to its strong UV-absorbing and emitting capabilities, high quantum yields, and general insensitivity to various chemical environments such as solution pH and solvent polarity.[6] Not surprisingly, BODIPYs are also pursued for a myriad of optoelectronic applications[7] in their own right, as well as molecular and ionic sensors and as stains for biological markers or dyes.[8] Very recently, ethynylated BODIPYs were successfully fused together to form dimeric and trimeric annulenes[9] that were determined to possess

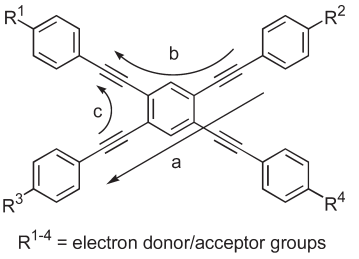

Figure 1. Conjugated pathways present in TAEB compounds. Pathways a and c represent linear and bent conjugation pathways, respectively, whereas path b represents cross conjugation.

antiaromatic properties (24 and 36 π-electrons, respectively), which represents another intriguing area of research to us.[10] Here, we report the synthesis of six structurally isomeric donor/acceptor-functionalized TAEBs (**1**−**6**, Figure 2). For control purposes, two additional TAEBs (**7**−**8**) and three structurally related bis-(arylethynyl)benzene (BAEBs, **9**−**11**) containing only acceptors were also prepared. The electronic absorption and emission spectra as well as computational studies of each series were also examined for structure−property relationships.

RESULTS AND DISCUSSION

Synthesis. The general synthetic strategy for TAEBs **1**−**8** and BAEBs **9**−**11** relies heavily on successive Sonogashira cross-coupling reactions. Donor and acceptor fragments are attached to a central tetrahalobenzene ring in a stepwise fashion that takes advantage of the reactivity differences toward aryl bromides and

Received: March 5, 2011
Published: April 15, 2011

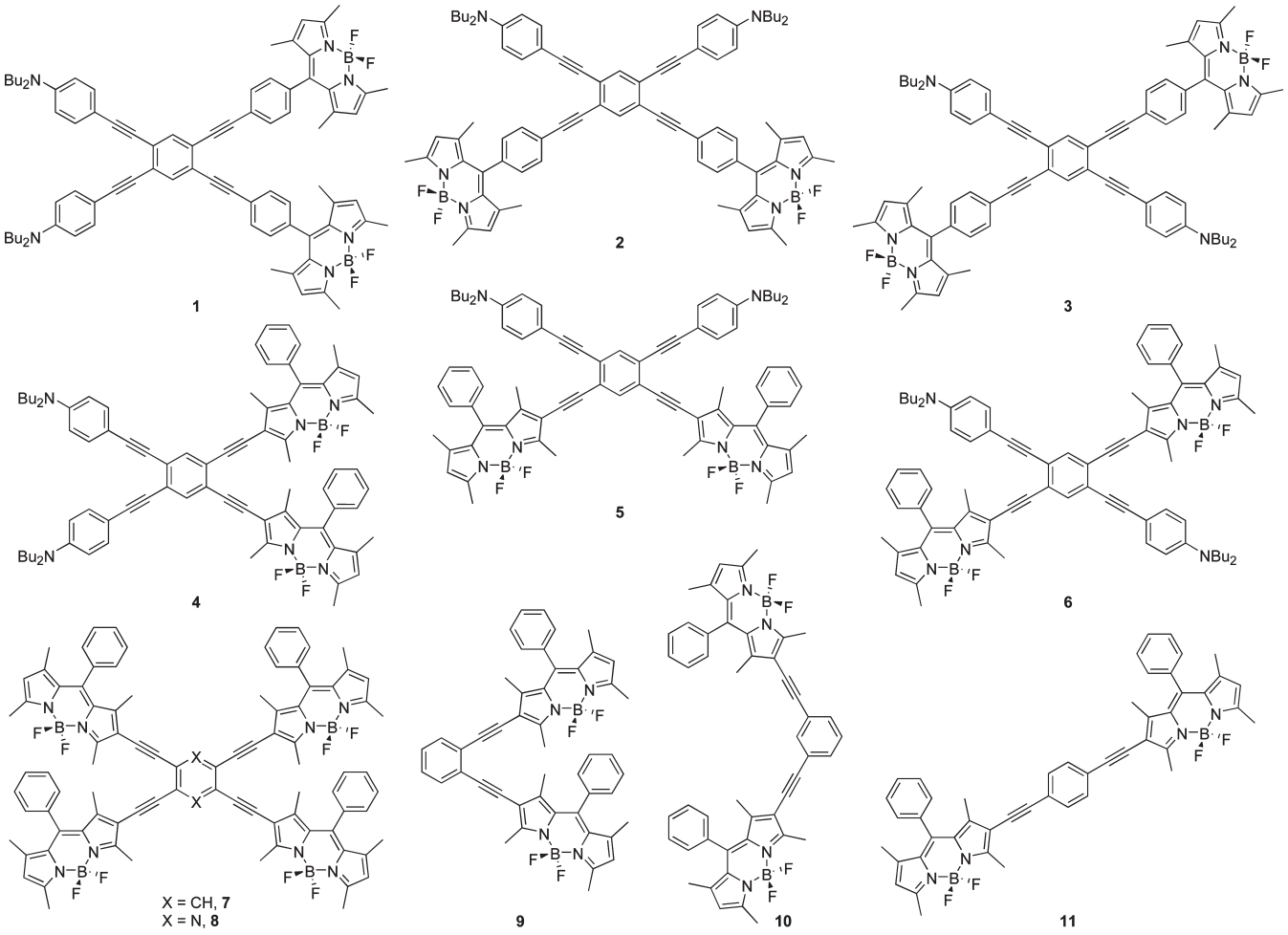

Figure 2. Target donor/acceptor-functionalized TAEBs **1**−**6**, all-acceptor TAEBs **7**−**8**, and BAEBs **9**−**11**.

Scheme 1. Synthesis of TAEBs 1−3

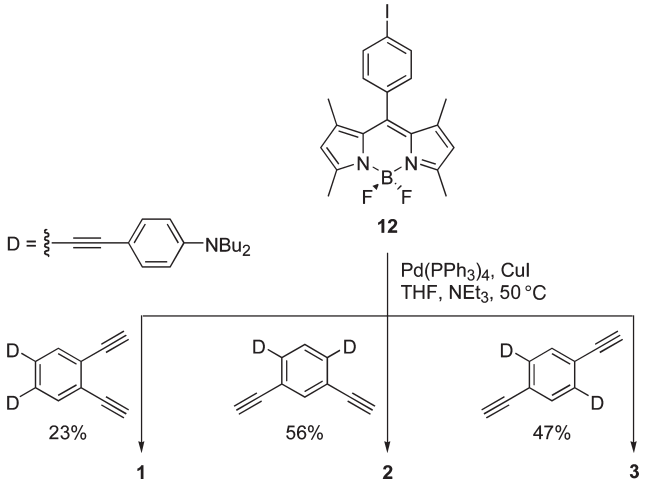

Scheme 2. Synthesis of BODIPY Precursor 16

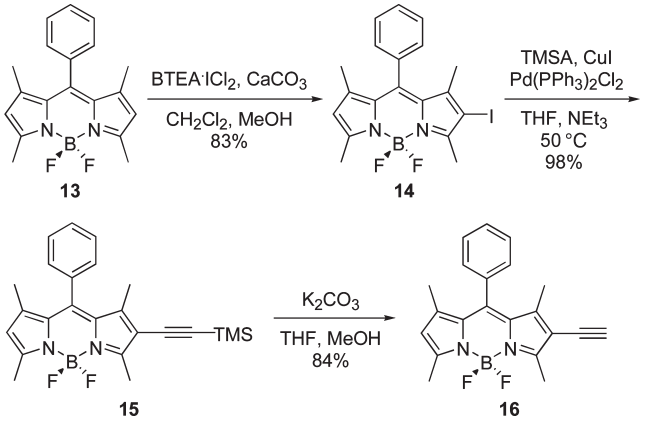

iodides in the catalytic cycle.[11] Specifically, cross-coupling of known iodide **12**[12] to the terminal alkynes of our previously reported bis(donor)-substituted precursors[3c] afforded TAEBs **1**−**3** as bright orange/red solids in low to moderate yield (Scheme 1).

To investigate isomeric TAEBs **4**−**8**, iodination of known precursor **13**[12b] furnished iodoBODIPY **14** (Scheme 2). Cross-coupling with (trimethylsilyl)acetylene (TMSA) provided silyl-protected **15** in high yield and subsequent desilylation afforded ethynylBODIPY **16**. The deprotection step should proceed no longer than 15 min as the B−F bonds undergo metathesis with

dx.doi.org/10.1021/jo200491m |*J. Org. Chem.* 2011, 76, 4043–4051

Scheme 3. Synthesis of TAEBs 4−6

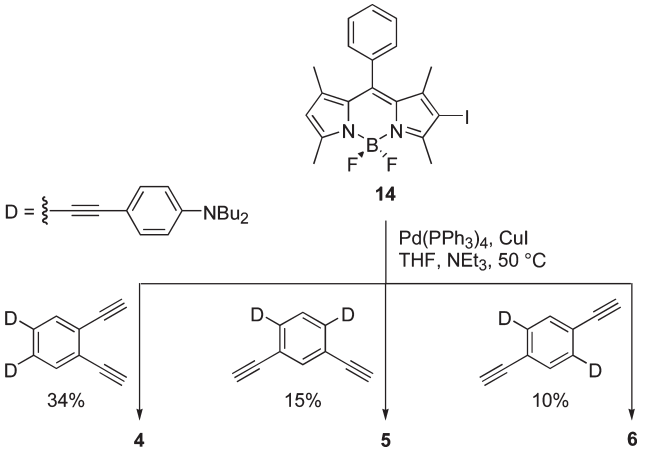

Scheme 4. Synthesis of TAEBs 7−8 and BAEBs 9−11

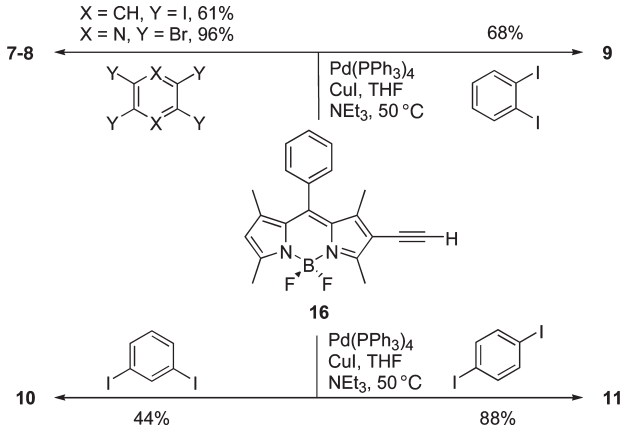

the excess methoxide to produce undesirable MeO-functionalized BODIPYs.[13] Despite this potential pitfall, **16** can be cleanly and efficiently synthesized in excellent overall yield.

Cross-coupling of **16** to the appropriate bis(donor)-substituted precursors[3c] afforded TAEBs **4**−**6** as bright red solids in low to modest yield (Scheme 3). We explored alternate routes (e.g., cross-coupling **16** with the appropriate bis(donor) dibromoarenes)[3c] and methods (e.g., Negishi-modified Sonogashira reaction),[14] but these variations worked no better.

Fortunately, no such problems for the synthesis of **7**−**8** were encountered. Specifically, cross-coupling ethynylBODIPY **16** with tetraiodobenzene or tetrabromopyrazine afforded all-acceptor TAEBs **7**−**8**, respectively (Scheme 4). Similarly, **16** was cross-coupled with 1,2-, 1,3- and 1,4-diiodobenzene to form related BAEBs **9**−**11**, respectively.

Electronic Absorption Spectra. The absorption spectra of **1**−**11** and **16** in toluene are shown in Figure 3; the data for both toluene and $CHCl_3$ are given in Table 1. All illustrate the characteristic pattern of two broad absorptions between 300 and 500 nm with extinction coefficients between 15 000 and 60 000 M^{-1} cm^{-1}, typical for intramolecular charge transfer bands in phenylacetylene scaffolds.[3] As seen with our previous systems,[3c,d] **1**−**11** follow the established trend for the longest λ_{max} in the high-energy region where the trend is ortho < meta < para with the para isomers exhibiting the most red-shifted charge

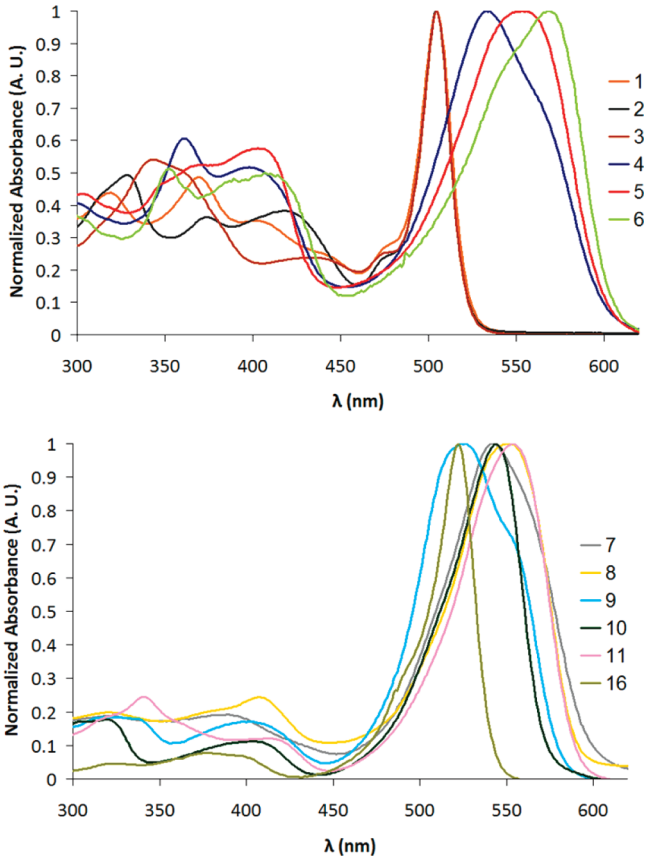

Figure 3. Electronic absorption spectra of (top) **1**−**6** and (bottom) **7**−**11**, **16** in toluene (PhMe); all spectra recorded at 10 μM concentration.

transfer band. For example, **1**−**3** display high-energy absorptions of 404, 423, and 443 nm, respectively, which are on par with TAEBs containing $-NO_2$ and $-CF_3$ groups. Isomers **4**−**6**, however, exhibit absorptions of 400, 402, and 412 nm, respectively, which are a considerably narrower range; similar absorptions are seen for **9**−**11** (398, 399, and 408 nm, respectively). Such behavior can be explained as a function of their attachment to the BODIPY core: while **1**−**3** are bound to the phenyl group on the meso position, **4**−**6** and **9**−**11** are bound directly to the electron-rich pyrrole. All-acceptors **7**−**8** and ethynylBODIPY **16** exhibit muted absorptions in this region due to either the lack of donor functionality (**7**−**8**) or conjugation altogether (**16**). However, **1**−**6** and **9**−**11** also possess an intense low-energy absorption, a trait not seen before in the TAEB scaffold. This low-energy absorption, attributable to the BODIPY acceptor unit, appears at ~505 nm for **1**−**3**, regardless of substitution pattern, presumably due to the fact that the acceptor unit is orthogonal to the π-system. A similar ortho < meta < para trend for the longest λ_{max} in the low-energy region with the para isomers exhibiting the most red-shifted absorption is observed for **4**−**6** and **9**−**11**. Isomers **4**−**6**, where the donor-functionalized phenylacetylene is directly linked to the BODIPY core, exhibit broad absorptions between 530 and 570 nm. Attachment of the acetylene to the acceptor unit does not induce the aforementioned rotational restrictions; therefore, full conjugation throughout the TAEB is permitted.[7h] Hence, placement of the phenylacetylene scaffold can have profound effects on the optical band gap as the lowest energy transition of **6** is 64 nm bathochromically shifted from **3** in

dx.doi.org/10.1021/jo200491m |J. Org. Chem. 2011, 76, 4043–4051

Table 1. Absorption and Emission Data for TAEBs 1−8, BAEBs 9−11, and EthynylBODIPY 16

		λ_{abs} (nm)					Stokes shift[c]			
entry	solvent	high-energy	low-energy	log(ε)[a]	λ_{em} (nm)	Φ_f (%)[b]	(nm)	(cm^{-1})	(nm)	(cm^{-1})
1	$CHCl_3$	404	502	5.07	520	4	116	5500	18	690
	PhMe	407	505	5.30	524	20	117	500	19	720
2	$CHCl_3$	423	503	4.92	518	4	95	4300	15	580
	PhMe	418	505	5.06	520	15	102	4700	15	570
3	$CHCl_3$	443	503	5.19	520	8	77	3300	17	640
	PhMe	438	505	5.06	520	15	82	3600	15	570
4	$CHCl_3$	400	533	4.91	606	<0.1	206	8500	73	2260
	PhMe	398	533	4.96	603	44	205	8500	70	2180
5	$CHCl_3$	402	553	4.96	608	<0.1	206	8400	55	1640
	PhMe	403	553	4.92	606	19	203	8300	53	1580
6	$CHCl_3$	412	564	4.77	602	<0.1	190	7700	38	1120
	PhMe	407	569	4.22	601	19	194	7900	32	940
7	$CHCl_3$	—[d]	540	5.33	590	54	—[d]	—[d]	50	1570
	PhMe	—[d]	542	4.66	591	74	—[d]	—[d]	49	1530
8	$CHCl_3$	—[d]	541	5.40	579	38	—[d]	—[d]	38	1210
	PhMe	—[d]	541	5.25	579	42	—[d]	—[d]	38	1210
9	$CHCl_3$	398	525	4.99	575	62	177	7700	50	1660
	PhMe	398	526	4.87	578	81	180	7800	52	1710
10	$CHCl_3$	399	542	5.04	569	78	170	7500	27	880
	PhMe	403	544	5.08	567	78	164	7200	23	750
11	$CHCl_3$	408	551	5.06	586	60	178	7400	35	1080
	PhMe	414	551	4.96	586	60	172	7100	35	1080
16	$CHCl_3$	—[d]	520	4.85	537	74	—[d]	—[d]	17	610
	PhMe	—[d]	522	4.89	539	72	—[d]	—[d]	17	600

[a] Determined from the low-energy absorption. [b] Quantum yields measured against an internal integrating sphere.[15] [c] Shifts determined as the difference between λ_{em} and high-energy λ_{abs}. [d] Not applicable.

toluene. All-acceptor **7** exhibits an absorption at 540 nm, which can be explained through similar means as **4**−**6**. Structurally related pyrazine **8** exhibits a similar shift at 541 nm, suggesting that variation of the central arene plays a minimal role in charge transfer. BAEBs **9**−**11** exhibit absorptions between 525 and 550 nm, which are hypsochromically shifted by 5−20 nm from **4**−**6**, rationalized from the lack of donor groups on the central arene. An approximate ratio exists between the extinction coefficients of the high and low-energy regions: for **1**−**6**, the ratio is 1:2 while for **9**−**11**, the ratio is 1:4. This can be rationalized by the simple comparison that **1**−**6** have twice the number of phenylacetylene groups bound to the central core than **9**−**11**. Also, the extinction coefficient for the low-energy absorption appears to be directly proportional to the number of acceptor groups present. For example, **1**−**6** and **9**−**11**, which have two acceptor groups, have low-energy extinction coefficients between 80 000 and 130 000 M^{-1} cm^{-1}, while **7** and **8** have approximate extinction coefficients of 210 000 and 250 000 M^{-1} cm^{-1}, respectively. No significant solvatochromic effects were observed for **1**−**11**, as the absorption spectra differed within 5 nm when compared to CH_2Cl_2 and toluene solutions.

Electronic Emission Spectra. The emission spectra for **1**−**11** and **16** in toluene are shown in Figure 4; the data for both toluene and $CHCl_3$ are given in Table 1. Perhaps the most striking feature is the lack of fluorescence solvatochromism: the largest deviation in emission λ_{max} is 4 nm in the entire series. While this phenomenon is regularly observed (with shifts as large as 65 nm) in the TAEB/BAEB architecture, it is completely absent in **1**−**11**, as is well-known for BODIPY molecules.[6] Positioning of the acceptor groups around the central arene also has little effect on the emission wavelengths: **1**−**3** all exhibit transitions near 520 nm regardless of substitution motif. Although this lack of differentiation is not unusual, typically seen by an 8−20 nm range between isomers where the difference increases in nonpolar solvents, **1**−**3** exhibit remarkably narrow difference of 2 nm. This trend is also observed with **4**−**6**, which exhibit emissions near 605 nm with a slightly larger deviation of 6 nm between isomers. The attachment point of the acceptor group, however, has a significant effect. As can be seen between **1**−**3** and **4**−**6**, the largest difference is observed between **2** and **5**, which possess emissions at 518 and 608 nm, respectively, where **5** demonstrates a 90 nm bathochromic shift from **2**. This behavior correlates well with anthracene/BODIPY systems developed by Burgess et al. where similar shifts were observed between like-systems.[7h] The emission for all-acceptors **7**−**8** were found at 590 and 579 nm, respectively, demonstrating that direct substitution of the two donors with an additional two acceptors results in a modest hypsochromic shift; however, **7**−**8** show a significant bathochromic shift compared to previously synthesized parent and tetra-donor TAEBs **17**−**18**,[3b] which suggests that an all-acceptor system may well outperform an all-donor one. Interestingly though, **9**−**11** emit between 570 and 590 nm, despite the lack of additional conjugation that **7**−**8** possess. Despite this, **9**−**11** follow the trend of meta < ortho < para with the para isomer

dx.doi.org/10.1021/jo200491m |J. Org. Chem. 2011, 76, 4043–4051

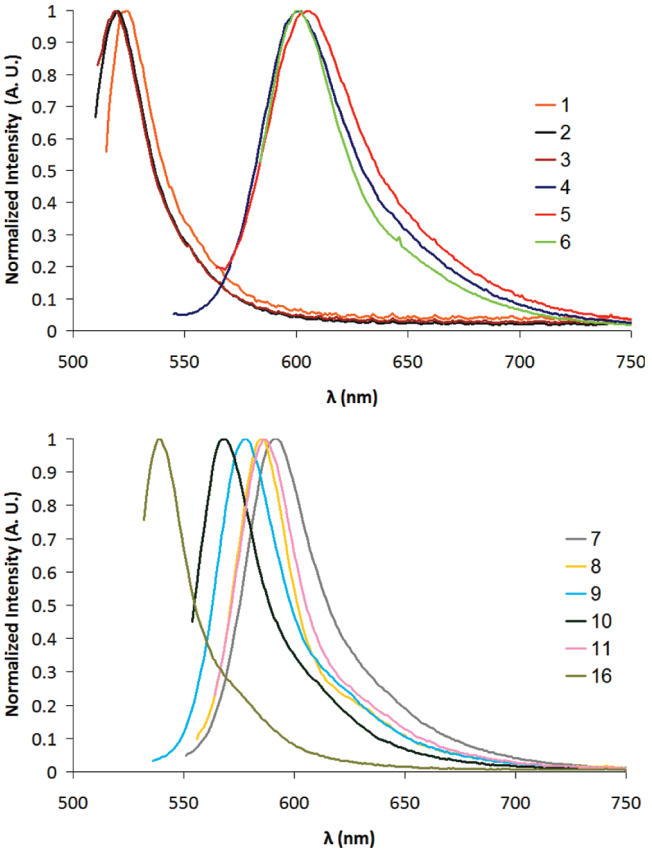

Figure 4. Emission spectra of (top) **1**−**6** and (bottom) **7**−**11**, **16** in toluene (PhMe); all spectra recorded at 10 μM concentration.

having the longest emission λ_{max}. Due to the fact that the emissions of **1**−**3** and **4**−**6** are within a narrow region, it is difficult to discern whether each series follows this trend; however, in terms of Stokes shifts, both **1**−**6** and **9**−**11** follow the previously established trend of para < meta < ortho, where the ortho isomer possess the largest dipole moment and hence the largest shift.

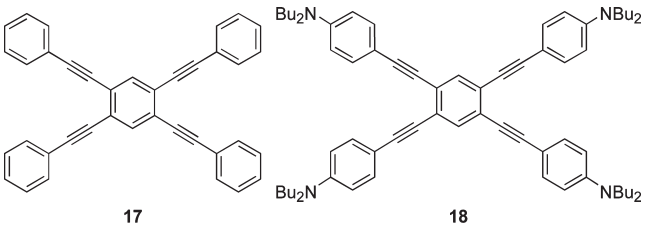

17 **18**

The fluorescence quantum yields were measured against an internal integrating sphere and the values reported in both $CHCl_3$ and toluene in Table 1.[15] In each instance, the Φ_f values were lower in $CHCl_3$ than in toluene. This holds specifically true for **4**−**6** where Φ_f values were nearly nonexistent in $CHCl_3$ while in toluene, Φ_f values were as high as 0.81 for **9**. In toluene, the general isomer trend was para < meta < ortho, the exact opposite found for pyridyl-functionalized systems. Furthermore, the CF_3-functionalized species afforded yet another order, suggesting that no broad generalizations for fluorescence quantum yields can be made for TAEBs/BAEBs.

Molecular Orbital Plots. Representative molecular orbital plots of the *ortho*-substituted systems **1**′, **4**′, and **9** along with all-acceptor **7** are shown in Figure 5, with the corresponding plots for **2**′−**3**′, **5**′−**6**′, **8**, and **10**−**11** in the Supporting Information. Structures **1**′−**6**′ are simplified by the replacement of NBu_2 groups with NMe_2 and all calculations are done on the B3LYP/6-31G* level of theory.[16] As seen with our previously synthesized TAEBs,[3c] the FMO plots of **1**′ and **4**′ indicate that the majority of density of the highest occupied molecular orbital (HOMO) resides on the donor end of the molecule, while the majority of density of the lowest unoccupied molecular orbital (LUMO) resides on the acceptor, indicative of charge-transfer processes. However, the majority of LUMO density resides on the acceptor moiety itself, leaving very little on the neighboring acetylenes and central arene; hence, the acceptor group is expected to be the dominant factor in any electronic transitions. This is chiefly observed with **1**′−**3**′ as all the LUMO density is found on the acceptor unit, which is situated orthogonally from the remainder of the phenylacetylene scaffold, thereby eliminating any possible overlap. Such behavior justifies the nearly identical emission profiles of **1**−**3** in Figure 4, which closely resemble **12**.[12a] The remaining compounds avoid this orthogonality issue. By attaching the acetylenes directly to one of the pyrrole units of the acceptor core, this leads essentially to coplanarity of the aromatic groups within TAEBs/BAEBs **4**−**11** as illustrated in the calculations as well as an X-ray structure for **8** (see Supporting Information). Therefore, **4**−**6** exhibit significantly red-shifted emission wavelengths with respect to **1**−**3**, that is, **4**−**6** maintain good intramolecular charge transfer while in full-conjugation with the phenylacetylene scaffold. Like **1**′−**6**′, the majority of LUMO density for **7**−**11** resides on the acceptor unit; however, the HOMO density for **7** and **9** extends throughout the entire molecule. As such, there is considerable overlap between their respective HOMO and LUMOs which give rise to $\pi-\pi^*$ transitions, similarly observed with **17**−**18**.[3b] The emission wavelengths of **7**−**11** confirm this assessment as their transitions are hypsochromically shifted as much as 40 nm with respect to **4**−**6**.

CONCLUSIONS

Donor/acceptor-functionalized TAEBs **1**−**6** as well as TAEBs **7**−**8** and structurally related BAEBs **9**−**11** containing only acceptors were synthesized and characterized. As such, these molecules displayed an array of intriguing optical properties that can be fine-tuned via small isomeric and structural variations. This especially holds true through comparison of **1**−**3** and **4**−**6**. All-acceptors **7**−**8** and related **9**−**11** also demonstrate the necessity for strong donors to ensure efficient charge transfer pathways. Despite the duality-imposed nature of **1**−**6** and **9**−**11**, all were shown to follow the previously established trends with respect to absorption and emission. However, the BODIPY acceptor was found to have a remarkable impact on the overall phenylacetylene scaffold such as its inability to exhibit any form of solvatochromism, a trend most often found in these systems. Furthermore, in some instances, despite the tendency to quench in polar solvents, the BODIPY unit was able to enhance the quantum yields to levels not yet seen with the TAEB molecules.

EXPERIMENTAL SECTION

General Comments. ^1H and ^{13}C NMR spectra were recorded in $CDCl_3$ or CD_2Cl_2 using either a 300 (^1H 299.93 MHz, ^{13}C 75.42 MHz)

dx.doi.org/10.1021/jo200491m |J. Org. Chem. 2011, 76, 4043–4051

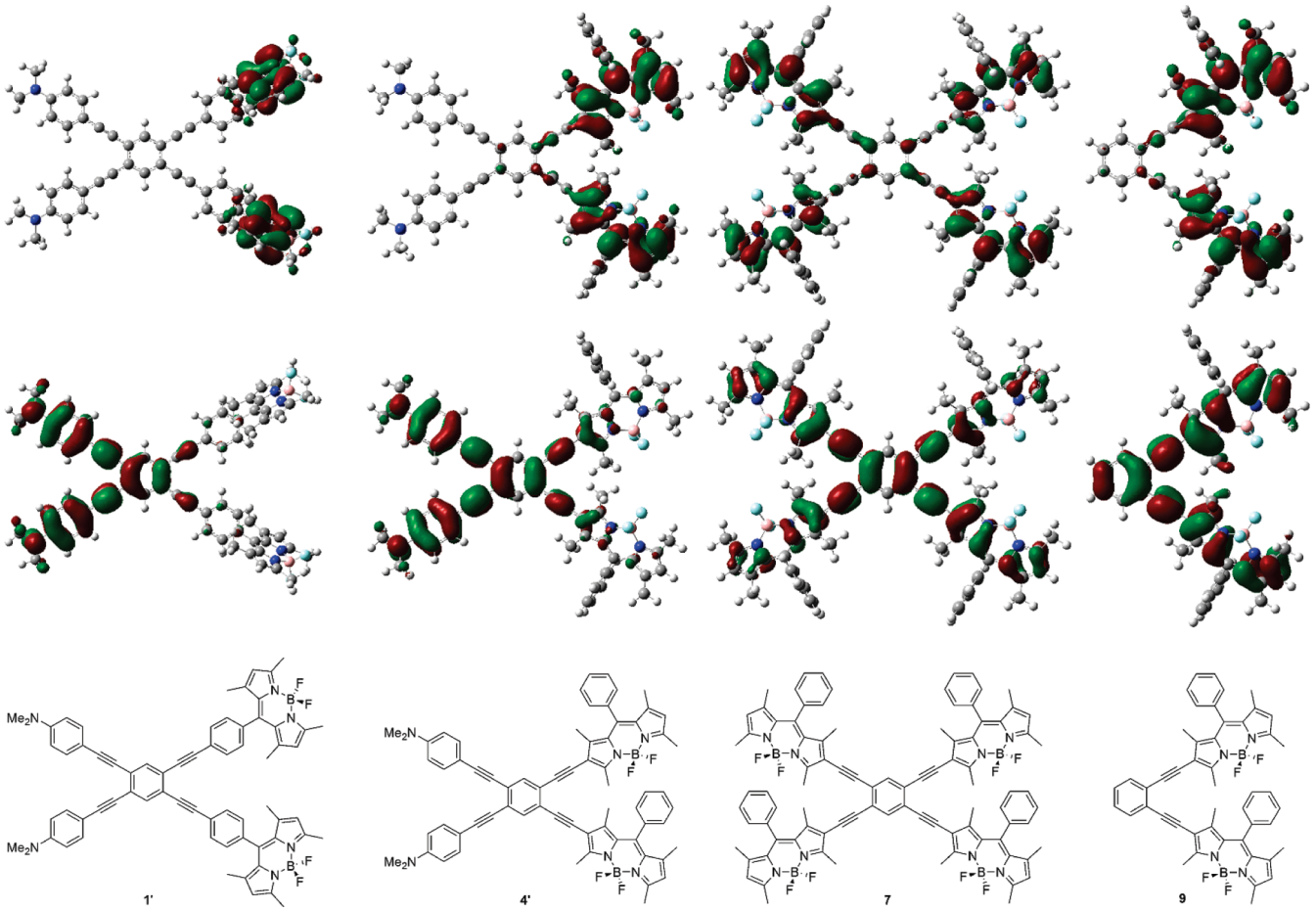

Figure 5. Representative molecular orbital plots (B3LYP/6-31G*) of simplified **1′**, **4′**, **7**, and **9**.[16] The lower plots represent the HOMOs while the upper plots represent the LUMOs.

or 500 MHz (^{1}H 500.11 MHz, ^{13}C 125.75 MHz) NMR spectrometer. Chemical shifts (δ) are expressed in ppm relative to the residual chloroform (^{1}H 7.27 ppm, ^{13}C 77.2 ppm) or dichloromethane (^{1}H 5.32 ppm, ^{13}C 54.0 ppm) reference. Coupling constants are expressed in hertz. IR spectra were recorded using a FTIR 550 spectrometer. UV−vis spectra were recorded on an UV−vis spectrometer. Fluorescence spectra and quantum yields were recorded on a spectrofluorimeter. High resolution mass spectra were recorded on a MALDI mass spectrometer. THF and CH_2Cl_2 were distilled from their appropriate drying agents under N_2. Unless otherwise stated, all reagents were purchased and used as received. Donor-functionalized phenylacetylenes as well as BODIPYs **12**−**13** were prepared by the respective previously reported methods.[3c,12]

IodoBODIPY 14. TetramethylBODIPY **13** (0.400 g, 1.23 mmol) and $CaCO_3$ (0.185 g, 1.85 mmol) were added to CH_2Cl_2 (100 mL), and MeOH (20 mL). BTEA·ICl_2 (0.480 g, 1.23 mmol) was then added and the mixture was stirred at rt for 1 h. After completion, the solution was evaporated to dryness. The crude material was chromatographed over silica gel (7:3 hexanes/CH_2Cl_2) to give **14** (0.460 g, 83%) as a red crystalline solid. ^{1}H NMR (CD_2Cl_2): δ 7.53−7.51 (m, 3H), 7.29−7.27, (m, 2H), 6.09 (s, 1H), 2.60 (s, 3H), 2.54 (s, 3H), 1.40 (s, 6H). ^{13}C NMR (CD_2Cl_2): δ 158.5, 154.7, 146.1, 143.8, 142.4, 135.3, 132.5, 131.4, 129.9, 129.8, 128.5, 123.9, 122.9, 84.5, 17.0, 16.1, 15.1, 14.9. IR (NaCl, CH_2Cl_2) ν: 3054, 2987, 2306, 1540, 1421, 1305 cm. UV−vis ($CHCl_3$) λ_{max} (log ε): 518 (4.93) nm. Em. ($CHCl_3$) λ_{max}: 537 nm. HRMS (MALDI) for $C_{19}H_{18}BF_2IN_2$ [M^+]: calcd 450.0576, found 450.0559.

(Trimethylsilylethynyl)BODIPY 15. IodoBODIPY **14** (0.358 g, 0.795 mmol), $Pd(PPh_3)_2Cl_2$ (0.017 g, 0.024 mmol), and CuI (0.009 g, 0.048 mmol) were dissolved in THF (30 mL) and Et_3N (30 mL). The mixture was degassed with Ar for 45 min. TMSA (0.44 mL, 3.18 mmol) was added to the solution and the resulting mixture was stirred overnight at 50 °C. Upon completion, the mixture was evaporated to dryness and the crude product was dissolved in CH_2Cl_2 and then passed through a pad of silica to remove insoluble material. The filtrate was evaporated to dryness and the crude product was chromatographed on silica (1:1 hexanes/CH_2Cl_2) to give **15** (0.325 g, 98%) as a red crystalline solid. ^{1}H NMR (CD_2Cl_2): δ 7.52−7.50 (m, 3H), 7.28−7.26 (m, 2H), 6.06 (s, 1H), 2.62 (s, 3H), 2.54 (s, 3H), 1.47 (s, 3H), 1.40 (s, 3H), 0.23 (s, 9H). ^{13}C NMR ($CDCl_3$): δ 158.5, 156.9, 145.7, 143.8, 143.1, 135.2, 133.2, 130.6, 129.9, 129.8, 128.5, 122.8, 115.8, 101.5, 98.2, 15.1, 14.9, 13. 8, 13.5, 0.5. IR (NaCl, CH_2Cl_2) ν: 3054, 2987, 2305, 2149, 1541, 1422, 1313 cm^{-1}. UV−vis ($CHCl_3$) λ_{max} (log ε): 529 (4.74) nm. Em. ($CHCl_3$) λ_{max}: 547. HRMS (MALDI) for $C_{24}H_{27}BF_2N_2Si$ [M^+]: calcd 420.2005, found 420.1991.

EthynylBODIPY 16. (Trimethylsilylethynyl)BODIPY **15** (0.460 g, 1.09 mmol) and K_2CO_3 (1.51 g, 10.9 mmol) were dissolved in THF (30 mL) and MeOH (30 mL) and then stirred for 15 min. The product mixture was evaporated to dryness, and the crude product was dissolved in CH_2Cl_2 and then passed through a pad of silica to remove excess K_2CO_3. The filtrate was evaporated to dryness and the crude product was chromatographed on silica (1:1 hexanes/CH_2Cl_2) to give **16** (0.292 g, 84%) as a red crystalline solid. ^{1}H NMR (CD_2Cl_2): δ 7.53−7.50 (m, 3H), 7.28−7.26 (m, 2H), 6.08 (s, 1H), 3.37 (s, 1H), 2.62 (s, 3H),

dx.doi.org/10.1021/jo200491m |*J. Org. Chem.* 2011, 76, 4043–4051

2.55 (s, 3H), 1.47 (s, 3H), 1.41 (s, 3H). ^{13}C NMR (CD_2Cl_2): δ 158.9, 156.6, 146.0, 144.0, 143.1, 135.0, 133.2, 130.3, 129.9, 129.8, 128.4, 122.9, 114.3, 84.0, 76.8, 15.1, 14.9, 13.6, 13.3. IR (NaCl, CH_2Cl_2) ν: 3052, 2987, 2152, 2062, 1485, 1464, 1382 cm^{-1}. UV−vis (toluene) λ_{max} (log ε): 522 (4.89) nm. Em. (toluene) λ_{max}: 539 nm. HRMS (MALDI) for $C_{21}H_{19}BF_2N_2$ [M$^+$]: calcd 348.1609, found 348.1623.

General Procedure for TAEB/BAEB Synthesis. BODIPY **12** or **14** was dissolved in THF (20 mL) and degassed with Ar for 45 min. In a separate flask, the appropriate diethynylarene, $Pd(PPh_3)_4$, and CuI were dissolved in THF (25 mL) and Et_3N (25 mL) and also degassed with Ar for 45 min. The solution containing **12** or **14** was then transferred by cannula into the second flask and the mixture was heated at 60 °C for 18−48 h. After cooling, the mixture was evaporated to dryness and the crude product was dissolved in CH_2Cl_2 and then passed through a pad of silica to remove insoluble material. The filtrate was evaporated to dryness and subsequently chromatographed on silica (1:1 CH_2Cl_2/hexanes) to afford the appropriate TAEB/BAEB derivative.

***ortho*-D/A-TAEB 1.** Following the general procedure, **12** (0.101 g, 0.224 mmol), 1,2-diethynyl-4,5-bis[(4′-*N*,*N*-dibutylaminophenyl)ethynyl]benzene[3c] (0.060 g, 0.102 mmol), $Pd(PPh_3)_4$ (0.007 g, 0.006 mmol), and CuI (0.007 g, 0.012 mmol) were reacted for 48 h. Chromatography on silica (1:1 CH_2Cl_2/hexanes) gave **1** (0.030 g, 23%) as a red/orange solid. ^{1}H NMR ($CDCl_3$): δ 7.74 (s, 2H), 7.70 (d, J = 8.7 Hz, 4H), 7.44 (d, J = 8.7 Hz, 4H), 7.30 (d, J = 8.7 Hz, 4H), 6.61 (d, J = 8.7 Hz, 4H), 6.00 (s, 4H), 3.32 (t, J = 7.2 Hz, 8H), 2.56 (s, 12H), 1.62−1.56 (m, 8H), 1.44 (s, 12H), 1.42−1.36 (m, 8H), 0.98 (t, J = 7.2 Hz). ^{13}C NMR ($CDCl_3$): δ 156.0, 148.5, 143.1, 140.8, 135.5, 134.7, 133.4, 132.5, 131.4, 128.5, 126.6, 124.2, 123.7, 121.7, 111.4, 108.6, 98.1, 94.0, 89.6, 86.2, 50.9, 29.6, 20.5, 14.8, 14.2. IR (NaCl, CH_2Cl_2) ν: 3054, 2987, 2305, 2194, 1605, 1547, 1523, 1513, 1471, 1307, 1270 cm^{-1}. UV−vis (toluene) λ_{max} (log ε): 505 (5.30) nm. Em. (toluene) λ_{max}: 524 nm. HRMS (MALDI) for $C_{80}H_{82}B_2F_4N_6$ [M$^+$]: calcd 1224.6723, found 1224.6744.

***meta*-D/A-TAEB 2.** Following the general procedure, **12** (0.101 g, 0.224 mmol), 1,5-diethynyl-2,4-bis[(4′-*N*,*N*-dibutylaminophenyl)ethynyl]benzene[3c] (0.060 g, 0.102 mmol), $Pd(PPh_3)_4$ (0.007 g, 0.006 mmol), and CuI (0.007 g, 0.012 mmol) were reacted for 48 h. Chromatography on silica (1:1 CH_2Cl_2/hexanes) gave **2** (0.030 g, 23%) as a red/orange solid. ^{1}H NMR ($CDCl_3$): δ 7.75−7.72 (m, 6H), 7.40 (d, J = 8.7 Hz, 4H), 7.32 (d, J = 8.7 Hz, 4H), 6.57 (d, J = 8.7 Hz, 4H), 6.01 (s, 4H), 3.30 (t, J = 7.2 Hz, 8H), 2.58 (s, 12H), 1.62−1.56 (m, 8H), 1.48 (s, 12H), 1.42−1.34 (m, 8H), 0.96 (t, J = 7.2 Hz, 12H). ^{13}C NMR ($CDCl_3$): δ 156.0, 148.7, 143.3, 141.1, 135.4, 135.0, 134.3, 133.4, 132.7, 131.5, 128.5, 127.3, 124.5, 123.2, 121.6, 111.4, 108.4, 98.3, 94.1, 89.9, 86.1, 51.0, 29.6, 20.6, 14.9, 14.2. IR (NaCl, CH_2Cl_2) ν: 3054, 2987, 2194, 1606, 1547, 1523, 1469, 1404, 1370, 1307, 1270 cm^{-1}. UV−vis (toluene) λ_{max} (log ε): 505 (5.06) nm. Em. (toluene) λ_{max}: 520 nm. HRMS (MALDI) for $C_{80}H_{82}B_2F_4N_6$ [M$^+$]: calcd 1224.6723, found 1224.6741.

***para*-D/A-TEAB 3.** Following the general procedure, **12** (0.101 g, 0.224 mmol), 1,4-diethynyl-2,5-bis[(4′-*N*,*N*-dibutylaminophenyl)ethynyl]benzene[3c] (0.060 g, 0.102 mmol), $Pd(PPh_3)_4$ (0.007 g, 0.006 mmol), and CuI (0.007 g, 0.012 mmol) were reacted for 48 h. Chromatography on silica (1:1 CH_2Cl_2/hexanes) gave **3** (0.030 g, 23%) as a red/orange solid. ^{1}H NMR ($CDCl_3$): δ 7.74 (d, J = 8.7 Hz, 4H), 7.73 (s, 2H), 7.40 (d, J = 8.7 Hz, 4H), 7.32 (d, J = 8.7 Hz, 4H), 6.57 (d, J = 8.7 Hz, 4H), 6.01 (s, 4H), 3.30 (t, J = 7.2 Hz, 8H), 2.58 (s, 12H), 1.62−1.56 (m, 8H), 1.48 (s, 12H), 1.42−1.34 (m, 8H), 0.96 (t, J = 7.2 Hz, 12H). ^{13}C NMR ($CDCl_3$): δ 155.9, 148.6, 143.3, 141.1, 135.4, 134.6, 133.3, 132.7, 131.4, 128.5, 125.8, 124.6, 124.4, 121.6, 111.4, 108.4, 97.8, 94.3, 89.8, 86.0, 50.9, 29.6, 20.5, 14.9, 14.2. IR (NaCl, CH_2Cl_2) ν: 3055, 2958, 2305, 2196, 1604, 1547, 1523, 1471, 1422, 1370, 1307 cm^{-1}. UV−vis (toluene) λ_{max} (log ε): 505 (5.06) nm. Em. (toluene) λ_{max}: 520 nm. HRMS (MALDI) for $C_{80}H_{82}B_2F_4N_6$ [M$^+$]: calcd 1224.6723, found 1224.6767.

***ortho*-D/A-TAEB 4.** Following the general procedure, **14** (0.050 g, 0.145 mmol), 1,2-diethynyl-4,5-bis[(4′-*N*,*N*-dibutylaminophenyl)ethynyl]benzene[3c] (0.050 g, 0.072 mmol), $Pd(PPh_3)_4$ (0.006 g, 0.004 mmol), and CuI (0.002 g, 0.008 mmol) were reacted for 48 h. Chromatography on silica (4:1 toluene/cyclohexane) gave **4** (0.031 g, 34%) as a red solid. ^{1}H NMR ($CDCl_3$): δ 7.58 (s, 2H), 7.50−7.48 (m, 6H), 7.40 (d, J = 8.7 Hz, 4H), 7.29 (m, 4H), 6.57 (d, J = 8.7 Hz, 4H), 6.05 (s, 2H), 3.29 (t, J = 7.2 Hz, 8H), 2.63 (s, 6H), 2.61 (s, 6H), 1.60−1.56 (m, 8H), 1.42 (s, 6H), 1.40 (s, 6H), 1.40−1.36 (m, 8H), 1.04 (t, J = 7.2 Hz, 12 H). ^{13}C NMR (CD_2Cl_2): δ 158.9, 156.9, 149.1, 145.8, 143.3, 143.0, 135.1, 134.8, 133.6, 129.9, 129.8, 129.8, 129.7, 128.5, 125.9, 124.5, 122.8, 111.8, 111.7, 108.6, 97.8, 94.9, 88.0, 86.5, 30.28, 29.9, 20.7, 15.1, 14.9, 14.5, 14.3, 13.9, 13.5. IR (NaCl, CH_2Cl_2) ν: 3054, 2987, 2360, 2149, 1539, 1521, 1313, 1193 cm^{-1}. UV−vis (toluene) λ_{max} (log ε): 533 (4.91) nm. Em. (toluene) λ_{max}: 603 nm. HRMS (MALDI) for $C_{80}H_{82}B_2F_4N_6$ [M$^+$]: calcd 1224.6723, found 1224.6704.

***meta*-D/A-TEAB 5.** Following the general procedure, **14** (0.050 g, 0.145 mmol), 1,5-diethynyl-2,4-bis[(4′-*N*,*N*-dibutylaminophenyl)ethynyl]benzene[3c] (0.050 g, 0.072 mmol), $Pd(PPh_3)_4$ (0.006 g, 0.004 mmol), and CuI (0.002 g, 0.008 mmol) were reacted for 48 h. Chromatography on silica (4:1 toluene/cyclohexane) gave **5** (0.013 g, 15%) as a red solid. ^{1}H NMR (CD_2Cl_2): δ 7.61 (s, 1H), 7.54 (s, 1H), 7.52−7.50 (m, 6H), 7.36−7.32 (m, 4H), 7.26 (d, J = 8.7 Hz, 4H), 6.55 (d, J = 8.7 Hz, 4H), 6.09 (s, 2H), 3.31 (t, J = 7.2 Hz, 8H), 2.68 (s, 6H), 2.55 (s, 6H), 1.63−1.56 (m, 8H), 1.53 (s, 6H), 1.42 (s, 6H), 1.39 (q, J = 6.5 Hz, 8H), 0.98 (t, J = 7.2 Hz, 12H). ^{13}C NMR (CD_2Cl_2): δ 158.5, 156.9, 148.9, 145.7, 143.5, 142.9, 135.3, 135.1, 134.8, 133.6, 129.8, 129.7, 128.5, 125.6, 124.1, 122.7, 111.6, 108.3, 97.6, 95.1, 88.0, 86.3, 51.2, 29.8, 20.9, 15.1, 14.9, 14.3, 14.0, 13.7. IR (NaCl, CH_2Cl_2) ν: 3054, 2960, 2198, 1539, 1520, 1264 cm^{-1}. UV−vis (toluene) λ_{max} (log ε): 553 (4.92) nm. Em. (toluene) λ_{max}: 606 nm. HRMS (MALDI) for $C_{80}H_{82}B_2F_4N_6$ [M$^+$]: calcd 1224.6723, found 1224.6696.

***para*-D/A-TAEB 6.** Following the general procedure, **14** (0.050 g, 0.145 mmol), 1,4-diethynyl-2,5-bis[(4′-*N*,*N*-dibutylaminophenyl)ethynyl]benzene[3c] (0.050 g, 0.072 mmol), $Pd(PPh_3)_4$ (0.006 g, 0.004 mmol), and CuI (0.002 g, 0.008 mmol) were reacted for 48 h. Chromatography on silica (4:1 toluene/cyclohexane) gave **6** (0.009 g, 10%) as a red solid. ^{1}H NMR (CD_2Cl_2): δ 7.59 (s, 2H), 7.53−7.50 (m, 6H), 7.36−7.32 (m, 4H), 7.26 (d, J = 8.7 Hz, 4H), 6.56 (d, J = 8.7 Hz, 4H), 6.09 (s, 2H), 3.31 (t, J = 7.5 Hz), 2.69 (s, 6H), 2.55 (s, 6H), 1.63−1.56 (m, 8H), 1.54 (s, 6H), 1.42 (s, 6H), 1.39 (q, J = 6.5 Hz, 8H), 0.99 (t, J = 7.2 Hz). ^{13}C NMR (CD_2Cl_2) δ 158.5, 156.8, 149.0, 145.8, 142.9, 135.1, 133.6, 129.8, 129.7, 129.5, 128.5, 127.3, 126.5, 124.8, 122.8, 114.3, 111.7, 110.5, 110.57, 110.55, 108.3, 97.4, 95.2, 88.2, 86.2, 51.2, 30.3, 29.5, 20.9, 4.9, 14.5, 14.4, 14.3, 13.7. IR (NaCl, CH_2Cl_2) ν: 3054, 2987, 2929, 2359, 1270 cm^{-1}. UV−vis (toluene) λ_{max} (log ε): 569 (4.77) nm. Em. (toluene) λ_{max}: 601 nm. HRMS (MALDI) for $C_{80}H_{82}B_2F_4N_6$ [M$^+$]: calcd 1224.6723, found 1224.6743.

tetra-A-TAEB 7. Following the general procedure, **16** (0.177 g, 0.508 mmol), 1,2,4,5-tetraiodobenzene (0.074 g, 0.127 mmol), $Pd(PPh_3)_4$ (0.017 g, 0.015 mmol), and CuI (0.006 g, 0.030 mmol) were reacted for 18 h. Chromatography on silica (4:1 $CHCl_3$/toluene) gave **7** (0.066 g, 61%) as a red solid. ^{1}H NMR ($CDCl_3$): δ 7.53−7.49 (m, 14H), 7.29−7.27 (m, 8H), 6.07 (s, 4H), 2.62 (s, 24H), 1.43 (s, 12H), 1.39 (s, 12H). ^{13}C NMR ($CDCl_3$): δ 158.1, 156.7, 145.1, 143.1, 142.4, 135.0, 134.8, 132.8, 130.5, 129.5, 129.4, 128.0, 124.9, 122.4, 115.0, 94.3, 88.2, 15.0, 14.8, 13.8, 13.4. IR (NaCl, CH_2Cl_2) ν: 3054, 2987, 2305, 2203, 1541, 1421, 1270 cm^{-1}. UV−vis (toluene) λ_{max} (log ε): 542 (5.33) nm. Em. (toluene) λ_{max}: 591 nm. HRMS (MALDI) for $C_{90}H_{74}B_4F_8N_8$ [M$^+$]: calcd 1462.6281, found 1462.6247.

Pyrazine TAEB 8. Following the general procedure, **16** (0.133 g, 0.382 mmol), 1,2,4,5-tetrabromopyrazine (0.038 g, 0.096 mmol), $Pd(PPh_3)_4$ (0.013 g, 0.011 mmol), and CuI (0.005 g, 0.023 mmol) were reacted for 18 h. Chromatography on silica (4:1 $CHCl_3$/toluene) gave **8**

(0.131 g, 93%) as a red solid. ^{1}H NMR ($CDCl_3$): δ 7.49−7.45 (m, 12H), 7.29−7.25 (m, 8H), 6.09 (s, 4H), 2.62 (s, 24H), 1.43 (s, 12H), 1.39 (s, 12H). ^{13}C NMR ($CDCl_3$): δ 159.1, 157.0, 145.7, 143.6, 142.6, 138.7, 134.6, 133.2, 130.3, 129.5, 128.0, 122.9, 113.7, 93.0, 91.1, 15.1, 14.8, 13.9, 13.4. IR (NaCl, CH_2Cl_2) ν: 3055, 2927, 2195, 1557, 1547, 1536, 1404, 1309, 1270 cm^{-1}. UV−vis (toluene) λ_{max} (log ε): 541 (5.40) nm. Em. (toluene) λ_{max}: 579 nm. HRMS (MALDI) for $C_{88}H_{72}B_4F_8N_{10}$ [M^+]: calcd 1464.6186, found 1464.6172.

***ortho*-BAEB 9.** Following the general procedure, **16** (0.090 g, 0.259 mmol), 1,2-diiodobenzene (0.043 g, 0.129 mmol), $Pd(PPh_3)_4$ (0.007 g, 0.008 mmol), and CuI (0.002 g, 0.016 mmol) were reacted for 18 h. Chromatography on silica (7:3 CH_2Cl_2/hexanes) gave **9** (0.044 g, 44%) as a violet solid. ^{1}H NMR (CD_2Cl_2): δ 7.53−7.47 (m, 8H), 7.31−7.26 (m, 6H), 6.09 (s, 2H), 2.56 (s, 12H), 1.43 (s, 6H), 1.39 (s, 6H). ^{13}C NMR (CD_2Cl_2): δ 158.4, 156.6, 145.7, 143.2, 142.9, 135.0, 133.1, 132.2, 130.7, 129.8, 129.7, 128.4, 128.3, 126.0, 122.7, 115.3, 95.1, 86.6, 15.1, 14.9, 13.8, 13.4. IR (NaCl, CH_2Cl_2) ν: 3054, 2987, 2305, 2203, 1541, 1421, 1270 cm^{-1}. UV−vis (toluene) λ_{max} (log ε): 526 (4.87) nm. Em. (toluene) λ_{max}: 578 nm. HRMS (MALDI) for $C_{48}H_{40}B_2F_4N_4$ [M^+]: calcd 770.3375, found 770.3397.

***meta*-BAEB 10.** Following the general procedure, **16** (0.090 g, 0.259 mmol), 1,3-diiodobenzene (0.043 g, 0.129 mmol), $Pd(PPh_3)_4$ (0.009 g, 0.008 mmol), and CuI (0.003 g, 0.016 mmol) were reacted for 18 h. Chromatography on silica (3:2 CH_2Cl_2/hexanes) gave **10** (0.068 g, 68%) as a violet solid. ^{1}H NMR (CD_2Cl_2): δ 7.55−7.52 (m, 7H), 7.40−7.37 (m, 2H), 7.32−7.30 (m, 4H), 7.29−7.26 (m, 1H), 6.08 (s, 2H), 2.66 (s, 6H), 2.55 (s, 6H), 1.51 (s, 6H), 1.42 (s, 6H). ^{13}C NMR (CD_2Cl_2): δ 158.6, 156.6, 145.9, 143.3, 143.0, 135.1, 133.2, 131.1, 130.7, 129.9, 129.8, 129.1, 128.5, 128.4, 124.5, 122.8, 115.2, 94.6, 83.2, 15.1. 14.9. 13.8. 13.5. IR (NaCl, CH_2Cl_2) ν: 3054, 2987, 2305, 2203, 1541, 1421, 1270 cm^{-1}. UV−vis (toluene) λ_{max} (log ε): 544 (5.08) nm. Em. (toluene) λ_{max}: 567 nm. HRMS (MALDI) for $C_{48}H_{40}B_2F_4N_4$ [M^+]: calcd 770.3375, found 770.3347.

***para*-TEAB 11.** Following the general procedure, **16** (0.070 g, 0.201 mmol), 1,4-diiodobenzene (0.033 g, 0.100 mmol), $Pd(PPh_3)_4$ (0.007 g, 0.006 mmol), and CuI (0.002 g, 0.012 mmol) were reacted for 18 h. Chromatography on silica (1:1 CH_2Cl_2/hexanes) gave **11** (0.068 g, 88%) as a violet solid. ^{1}H NMR (CD_2Cl_2): δ 7.53−7.49 (m, 6H), 7.41 (s, 4H), 7.32−7.30 (m, 4H), 6.09 (s, 2H), 2.65 (s, 6H), 2.55 (s, 6H), 1.51 (s, 6H), 1.42 (s, 6H). ^{13}C NMR (CD_2Cl_2): δ 158.6, 156.6, 145.9, 143.2, 143.0, 135.1, 133.2, 131.6, 130.9, 129.9, 129.8, 128.5, 123.6, 122.8, 115.3, 96.2, 84.5, 15.1, 14.9, 13.8, 13.5. IR (NaCl, CH_2Cl_2) ν: 3054, 2987, 2305, 2203, 1541, 1421, 1270 cm^{-1}. UV−vis (toluene) λ_{max} (log ε): 554 (4.96) nm. Em. (toluene) λ_{max}: 586 nm. HRMS (MALDI) for $C_{48}H_{40}B_2F_4N_4$ [M^+]: calcd 770.3375, found 770.3336.

■ ASSOCIATED CONTENT

Supporting Information. Copies of ^{1}H and ^{13}C NMR spectra for **1**−**11** and **14**−**16**; molecular orbital plots for **1′**−**6′** and **7**−**11**; computational details for **1′**−**6′** and **7**−**11**; X-ray ORTEP plot and cif file for **8**. This material is available free of charge via the Internet at http://pubs.acs.org.

■ AUTHOR INFORMATION

Corresponding Author

*E-mail: haley@uoregon.edu.

■ ACKNOWLEDGMENT

We thank the National Science Foundation (CHE-1013032) for support of this research, as well as for support in the form of instrumentation grants (CHE-0639170 and CHE-0923589). We thank Dr. Lev Zakharov for obtaining the X-ray structure of **8**.

■ REFERENCES

(1) (a) de Meijere, A., Ed. *Carbon Rich Compounds I*; Topics in Current Chemistry; Springer: Berlin, 1998; Vol. 196. (b) de Meijere, A., Ed. *Carbon Rich Compounds II*; Topics in Current Chemistry; Springer: Berlin, 1999; Vol. 201. (c) Diederich, F., Stang, P. J., Tykwinski, R. R., Eds. *Acetylene Chemistry: Chemistry, Biology, and Material Science*; Wiley-VCH: Weinheim, 2005. (d) Haley, M. M., Tykwinski, R. R., Eds. *Carbon-Rich Compounds: From Molecules to Materials*; Wiley-VCH: Weinheim, 2006.

(2) Reviews, inter alia: (a) *Organic Light Emitting Devices: Synthesis, Properties and Applications*; Mullen, K., Scherf, U., Eds.; Wiley-VCH: Weinheim, 2006. (b) Chen, J.; Reed, M. A.; Dirk, S. M.; Price, D. W.; Rawlett, A. M.; Tour, J. M.; Grubisha, D. S.; Bennett, D. W. In *Molecular Electronics: Bio-Sensors and Bio-Computers*; NATO Science Series II: Mathematics, Physics, Chemistry; Plenum: New York, 2003; Vol. 96, pp 59−195. (c) Domerco, B.; Hreha, R. D.; Zhang, Y.-D.; Haldi, A.; Barlow, S.; Marder, S. R.; Kippelen, B. *J. Poly. Sci. Part B: Poly. Phys.* **2003**, *41*, 2726–2732. (d) Shirota, Y. *J. Mater. Chem.* **2000**, *10*, 1–25. (e) Schwab, P. F. H.; Levin, M. D.; Michl, J. *Chem. Rev.* **1999**, *99*, 1863–1933.(f) *Electronic Materials: The Oligomer Approach*; Mullen, K., Wegner, G., Eds.; Wiley-VCH: Weinheim, 1998. (g) *Nonlinear Optics of Organic Molecules and Polymers*; Nalwa, H. S., Miyata, S., Eds.; CRC Press: Boca Raton, FL, 1997.

(3) (a) Miller, J. J.; Marsden, J. A.; Haley, M. M. *Synlett* **2004**, 165–168. (b) Marsden, J. A.; Miller, J. J.; Shirtcliff, L. D.; Haley, M. M. *J. Am. Chem. Soc.* **2005**, *127*, 2464–2476. (c) Spitler, E. L.; Shirtcliff, L. D.; Haley, M. M. *J. Org. Chem.* **2007**, *72*, 86–96. (d) Spitler, E. L.; Monson, J. M.; Haley, M. M. *J. Org. Chem.* **2008**, *73*, 2211–2223. (e) Samori, S.; Tojo, S.; Fujitsuka, M.; Splitler, E. L.; Haley, M. M.; Majima, T. *J. Org. Chem.* **2007**, *72*, 2785–2793. (f) Samori, S.; Tojo, S.; Fujitsuka, M.; Splitler, E. L.; Haley, M. M.; Majima, T. *J. Org. Chem.* **2008**, *73*, 3551–3558.

(4) Inter alia: (a) Zucchero, A. J.; McGrier, P. A.; Bunz, U. H. F. *Acc. Chem. Res.* **2010**, *43*, 397–408. (b) Kang, H.; Zhu, P.; Yang, Y.; Facchetti, A.; Marks, T. J. *J. Am. Chem. Soc.* **2004**, *126*, 15974–15975. (c) Wilson, J. N.; Josowicz, M.; Wang, Y.; Bunz, U. H. F. *Chem. Commun.* **2003**, 2962–2963. (d) Wilson, J. N.; Hardcastle, K. I.; Josowicz, M.; Bunz., U. H. F. *Tetrahedron* **2004**, *60*, 7157–7167.

(5) (a) Huang, J.-H.; Sun, Y.-Y.; Chou, P. T.; Fang, J.-M. *J. Org. Chem.* **2005**, *70*, 5827–5832. (b) Wilson, J. N.; Bunz, U. H. F. *J. Am. Chem. Soc.* **2005**, *127*, 4124–4125. (c) Brombosz, S. M.; Zucchero, A. J.; Phillips, R. L.; Vazquez, D.; Wilson, A.; Bunz, U. H. F. *Org. Lett.* **2007**, *9*, 4519–4522. (d) Tolosa, J.; Zucchero, A. J.; Bunz, U. H. F. *J. Am. Chem. Soc.* **2008**, *130*, 6498–6506.

(6) (a) Loudet, A.; Burgess, K. *Chem. Rev.* **2007**, *107*, 4891–4932. (b) Ziessel., R.; Ulrich, G.; Harriman, A. *New. J. Chem.* **2007**, *31*, 496–501. (c) Ulrich, G.; Ziessel, R.; Harriman, A. *Angew. Chem., Int. Ed.* **2008**, *47*, 1184–1201.

(7) (a) Harriman, A.; Izzet, G.; Ziessel, R. *J. Am. Chem. Soc.* **2006**, *128*, 10868–10875. (b) Singh-Rachford, T. N.; Haefele, A.; Ziessel, R.; Castellano, F. N. *J. Am. Chem. Soc.* **2008**, *130*, 16164–16165. (c) Guliyev, R.; Coskun, A.; Akkaya, E. U. *J. Am. Chem. Soc.* **2009**, *131*, 9007–9013. (d) Harriman, A.; Mallon, L. J.; Elliot, K. J.; Haefele, A.; Ulrich, G.; Ziessel, R. *J. Am. Chem. Soc.* **2009**, *131*, 13375–13386. (e) Golovkova, T. A.; Kozlov, D. V.; Neckers, D. C. *J. Org. Chem.* **2005**, *70*, 5545–5549. (f) Goze, C.; Ulrich, G.; Ziessel, R. *J. Org. Chem.* **2007**, *72*, 313–322. (g) Zrig, S.; Rémy, P.; Andrioletti, B.; Rose, E.; Asselberghs, I.; Clay, K. *J. Org. Chem.* **2008**, *73*, 1563–1566. (h) Wan, C.-W.; Burghart, A.; Chen, J.; Berström, F.; Johansson, L. B.-Å.; Wolford, M. F.; Kim, T. G.; Topp, M. R.; Hochstrasser, R. M.; Burgess, K. *Chem.—Eur. J.* **2003**, *9*, 4430–4441. (i) Yilmaz, M. D.; Bozdemir, O. A.; Akkaya, E. U. *Org. Lett.* **2006**, *8*, 2871–2873. (j) Zhang, X.; Qian, X. *Org. Lett.* **2008**, *10*, 29–32. (k) Buyukcaki, O.; Bozdemir, O. A.; Kolemen, S.; Erbas, S.; Akkaya, E. U. *Org. Lett.* **2009**, *11*, 4644–4647. (l) Cakmak, Y.; Akkaya, E. U. *Org. Lett.* **2009**, *11*, 85–88.

(8) (a) Atilgan, S.; Ozdemir, T.; Akkaya, E. U. *Org. Lett.* **2008**, *10*, 4065–4067. (b) Ekmekci, Z.; Yilmaz, M. D.; Akkaya, E. U. *Org. Lett.* **2008**, *10*, 461–464. (c) Yuan, M.; Li, Y.; Li, J.; Li, C.; Liu, X.; Lv, J.; Xu, J.; Liu, H.; Wang, S.; Zhu, D. *Org. Lett.* **2007**, *9*, 2313–2316. (d) Gabe, Y.;

Urano, Y.; Kikuchi, K.; Kojima, H.; Nagano, T. *J. Am. Chem. Soc.* **2004**, *126*, 3357–3367. (e) Wu, L.; Loudet, A.; Barhoumi, R.; Burgardt, R. C.; Burgess, K. *J. Am. Chem. Soc.* **2009**, *131*, 9156–9157. (f) Sun, Z.-N.; Wang, H.-L.; Liu, F.-Q.; Chen, Y.; Tam, P. K. H.; Yang, D. *Org. Lett.* **2009**, *11*, 1887–1890. (g) Ziessel, R.; Ulrich, G.; Harriman, A.; Alamiry, M. A. H.; Steart, B.; Retailleau, P. *Chem.—Eur. J.* **2009**, *15*, 1359–1369. (h) Namkung, W.; Padmawar, P.; Mills, A. D.; Verkman, A. S. *J. Am. Chem. Soc.* **2008**, *130*, 7794–7795.

(9) Sakida, T.; Yamaguchi, S.; Shinokubo, H. *Angew. Chem., Int. Ed.* **2011**, *50*, 2280–2283.

(10) Spitler, E. S.; Johnson, C. A.; Haley, M. M. *Chem. Rev.* **2006**, *106*, 5344–5386.

(11) (a) Marsden, J. A.; Haley, M. M. In *Metal-Catalyzed Cross-Coupling Reactions*, 2nd ed.; de Meijere, A., Diederich, F., Eds.; Wiley-VCH: Weinheim, 2004; pp 317−394. (b) Sonogashira, K. In *Metal-Catalyzed Cross-Coupling Reactions*; Diederich, F., Stang, P. J., Eds.; Wiley-VCH: Weinheim, 1998; pp 203−230.

(12) (a) Burghart, A.; Kim, H.; Welch, M. B.; Thoreson, L. H.; Reibenspies, J.; Burgess, K. *J. Org. Chem.* **1999**, *64*, 7813–7819. (b) Singh-Rachfrod, T. N.; Haefele, A.; Ziessel, R.; Castellano, F. N. *J. Am. Chem. Soc.* **2008**, *130*, 16164–16165.

(13) (a) Gabe, Y.; Ueno, T.; Urano, Y.; Kojima, H.; Nagano, T. *Anal. Bioanal. Chem.* **2006**, *386*, 621–626. (b) L.; Liu, F.-Q.; Chen, Y.; Tam, P. K. H.; Yang, D. *Org. Lett.* **2009**, *11*, 1887–1890.

(14) (a) King, A. O.; Negishi, E.-I. *J. Org. Chem.* **1978**, *43*, 353–360. (b) Sonoda, M.; Inaba, A.; Itahashi, K.; Tobe, Y. *Org. Lett.* **2001**, *3*, 2419–2421.

(15) Porrès, L.; Holland, A.; Pålsson, L.-O.; Monkman, A. P.; Kemp, C.; Beeby, A. *J. Fluoresc.* **2006**, *16*, 267–272.

(16) Frisch, M. J.; Trucks, G. W.; Schlegel, H. B.; Scuseria, G. E.; Robb, M. A.; Cheeseman, J. R.; Montgomery, J. A. Jr.; Vreven, T.; Kudin, K. N.; Burant, J. C.; Millam, J. M.; Iyengar, S. S.; Tomasi, J.; Barone, V.; Mennucci, B.; Cossi, M.; Scalmani, G.; Rega, N.; Petersson, G. A.; Nakatsuji, H.; Hada, M.; Ehara, M.; Toyota, K.; Fukuda, R.; Hasegawa, J.; Ishida, M.; Nakajima, T.; Honda, Y.; Kitao, O.; Nakai, H.; Klene, M; Li, X.; Knox, J. E.; Hratchian, H. P.; Cross, J. B.; Adamo, C.; Jaramillo, J.; Gomperts, R.; Stratmann, R. E.; Yazyev, O.; Austin, A. J.; Cammi, R.; Pomelli, C.; Ochterski, J. W.; Ayala, P. Y.; Morokuma, K.; Voth, G. A.; Salvador, P.; Dannenberg, J. J.; Zakrzewski, V. G.; Dapprich, S.; Daniels, A. D.; Strain, M. C.; Farkas, O.; Malick, D. K.; Rabuck, A. D.; Raghavachari, K.; Foresman, J. B.; Ortiz, J. V.; Cui, Q.; Baboul, A. G.; Clifford, S.; Cioslowski, J.; Stefanov, B. B.; Liu, G.; Liashenko, A.; Piskorz, P.; Komaromi, I.; Martin, R. L.; Fox, D. J.; Keith, T.; Al-Laham, M. A.; Peng, C. Y.; Nanayakkara, A.; Challacombe, M.; Gill, P. M. W.; Johnson, B.; Chen, W.; Wong, M. W.; Gonzalez, C.; Pople, J. A. *Gaussian 03*, Revision B.04; Gaussian, Inc., Pittsburgh PA, 2003.